Ultra-narrow bandpass optical interference filters for deep space optical communication.

Thomas Rahmlow, Timothy Upton, Markus Fredell, Terry Finnell, Stephen Washkevich,
Kirk Winchester, Tina Hoppock and Robert Johnson
Omega Optical, Inc.
Brattleboro, Vermont

Proc. SPIE 10524, Free-Space Laser Communication and Atmospheric Propagation XXX, 1052416 (2018);
doi:10.1117/12.2290753

Copyright 2019 Society of Photo-Optical Instrumentation Engineers. One print or electronic copy may be made for personal use only. Systematic reproduction and distribution, duplication of any material in this paper for a fee or for commercial purposes, or modification of the content of the paper are prohibited.

High-speed multispectral confocal imaging

Gary E. Carver*[a], Sarah A. Locknar[a], William A. Morrison[a], Daniel L. Farkas[b]
[a]Omega Optical, 21 Omega Drive, Brattleboro, VT, USA 05301;
[b]Spectral Molecular Imaging, 250 N. Robertson Blvd., Beverly Hills, CA, USA 90211

Proc. SPIE 8587, Imaging, Manipulation, and Analysis of Biomolecules, Cells, and Tissues XI, 858715
(February 22, 2013); doi:10.1117/12.2001883

Copyright 2019 Society of Photo-Optical Instrumentation Engineers. One print or electronic copy may be made for personal use only. Systematic reproduction and distribution, duplication of any material in this paper for a fee or for commercial purposes, or modification of the content of the paper are prohibited.

High-speed multispectral confocal imaging

Gary E. Carver*[a], Sarah A. Locknar[a], William A. Morrison[a], Daniel L. Farkas[b]
[a]Omega Optical, 21 Omega Drive, Brattleboro, VT, USA 05301;
[b]Spectral Molecular Imaging, 250 N. Robertson Blvd., Beverly Hills, CA, USA 90211

ABSTRACT

A new approach for generating high-speed multispectral images has been developed. The central concept is that spectra can be acquired for each pixel in a confocal spatial scan by using a fast spectrometer based on optical fiber delay lines. This concept merges fast spectroscopy with standard spatial scanning to create datacubes in real time. The spectrometer is based on a serial array of reflecting spectral elements, delay lines between these elements, and a single element detector. The spatial, spectral, and temporal resolution of the instrument is described, and illustrated by multispectral images of laser-induced autofluorescence in biological tissues.

Keywords: Multispectral scanning, autofluorescence, tissue imaging, confocal

1. INTRODUCTION

Fast multispectral confocal mapping has great promise for imaging cancer at the tissue and cellular levels.[1] Biomedical researchers hope to detect tumor angiogenesis, take optical biopsies, perform treatments (including laser surgery and photodynamic therapy), and monitor long-term results. Ex-vivo studies can be performed on tissue samples labeled with various fluorescent dyes. The most likely in-vivo applications in humans should detect intrinsic signals such as autofluorescence. Often considered background noise that interferes with other signals, spectrally resolved autofluorescence provides a wealth of information regarding many metastases – including lung,[2,3] colorectal,[4] and breast cancers[5]. As an example, the fluorescence spectra of healthy tissue, metaplastic tissue, dysplastic tissue, and invasive carcinoma have been published.[2] These spectra indicate that ten wavelength bins distributed from 500 to 800 nm would easily distinguish amongst the various tissues, and allow for high specificity and sensitivity.

The above goals simultaneously require sufficient spatial, spectral, and temporal resolution. Confocal microscopy can map millimeter sized fields-of-view with ~ micron spatial resolution. Spectroscopic tools can provide multispectral data during laser excitation of fluorescence. Further, these spatial and spectral measurements should allow for the detection of millisecond dynamics in living systems. All of these characteristics are not yet available in one cost-effective instrument, mostly because the spectroscopic tools are not fast enough.

We present here a new approach for generating high-speed multispectral images of intrinsic fluorescence. The central concept is that spectra can be acquired for each pixel in a confocal spatial scan by using a fast spectrometer based on optical fiber delay lines. Since the spectrometer is fiber-based, the face of the entrance fiber can act as the pinhole in a confocal microscope. This concept merges fast spectroscopy with standard spatial scanning to create datacubes in real time. Originally considered for course wavelength division multiplexing at telecom wavelengths in the near infrared, this concept is a good match for applications that require 10 to 15 wavelength bins at visible and near infrared wavelengths. This project merges expertise from the telecommunications[6] and biomedical sectors.[7]

The following sections describe the design, attributes, performance and advantages of this new instrument. Examples are given of multispectral images taken on several samples - including fluorescent beads, quantum dots, fixed tissue, and ex-vivo tissue. Scans taken with an endoscopic bundle are also presented. This project was funded by the National Cancer Institute through the National Institutes of Health (SBIR Phase II grant number 5R44CA124036-03).

* gcarver@omegafilters.com; phone 1 802 251-7346; www.omegafilters.com

2. OPTICAL DESIGN

A schematic of our multispectral confocal scanner is shown in figure 1. The following sub-sections describe the confocal, endoscopic, and spectroscopic sub-systems.

2.1 Confocal scanner

As with fluorescence microscopes, our excitation beam enters the system by reflecting from a dichroic splitter. The excitation is provided by a pulsed 488 nm or 405 nm laser. Averaged over 1 second, excitation levels at the tissue are in the 1 to 2 milliwatt range. Optical power should be limited to about 5 milliwatts for operating room safety reasons and to avoid potential tissue damage[8] in the subject.

Confocal microscopes are widely available from several leading companies. The basic concept of confocal scanning is shown by the two scanning mirrors and associated optics in figure 1. As the two mirrors are scanned in an x-y raster pattern, the focused spot on the sample is always conjugate with a pinhole or small area detector (the pinhole in figure 1 is the fiber aperture marked with an asterisk). The pinhole limits the acceptance of light from axial and lateral locations away from the position of the focused spot. Since fluorescence from biological materials typically occurs within 1 to 5 nsec after excitation, both reflected and photoexcited signals propagate back to the pinhole before the mirrors can move appreciably. This allows the mirrors to de-scan back-propagating photons such that light from the focused spot indeed stays conjugate with the pinhole. As a result, scanning confocal systems can generate maps (or "images") with spatial resolution at or near the laser spot size. In this system, the 488 nm laser is focused at NA = 0.24 to a 1.2 micron diameter spot and scanned over an adjustable field (can be zoomed from 50 to 500 microns). Since the scanning process actually generates a spatial convolution of the focused spot with features in the sample, it is possible to detect features below the diffraction limit (though they appear equal in size to the spot). These ideas[9] have been applied to images of functional nuclear architecture[10], and have been used for years in the materials and semiconductor industries.[11]

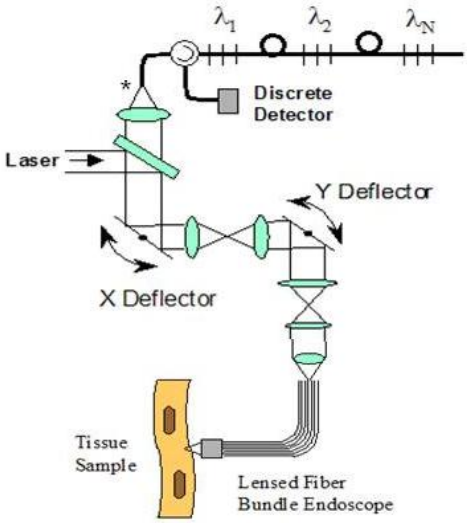

Figure 1. Multispectral confocal scanning system

2.2 Endoscopic optics

The system depicted in figure 1 performs microscopy when a sample is placed at the focus of the objective lens, and endoscopy when the proximal end of an endoscope is placed in the same location. For endoscopy, a coherent fiber bundle with 30,000 three micron diameter fibers is placed under the lens. The confocal scanner raster scans the proximal end of the endoscope. A given fiber within the bundle transfers the laser to the distal end where a lensed tip relays the beam from the fiber to the tissue. Fluorescence or reflected light from a resolution element is imaged back into the same

fiber, propagates back to the proximal end, is collected and de-scanned by the confocal optical system, and is finally focused on the confocal pinhole. This entire process occurs within the dwell time of the raster scan (2.5 microseconds in our design). During endoscopy, the 488 nm laser is focused by the distal tip at NA = 0.8 to a 0.4 micron diameter spot and scanned over an adjustable field at a working distance of 80 microns (can be zoomed from 10.8 to 108 microns). The transmission of this endoscope is consistent with reports in the literature.[12] The following sub-section describes our new spectrometer, which conveniently maps proximal reflection and emission bands into different temporal bins.

2.3 Fiber-optic spectrometer

Our fiber optic spectrometer is based on a serial array of reflecting spectral elements, delay lines between these elements, and a single element detector. After excitation by a laser pulse, broadband fluorescence from a biological tissue sample propagates into the array via the confocal aperture, light of the first wavelength band reflects from the first element, and light of the Nth wavelength band reflects from the Nth element. Each wavelength is mapped into a specific time slot. Each delay line is equal to the length of the laser pulse. The spectral elements can be fabricated in two ways - fiber tips can be coated with interference filters to create > 10 nm wide spectral slices, while fiber Bragg gratings can be written into the fiber core to create 1 to 2 nm wide spectral slices[13]. Most spectrometers employ one grating that disperses light spatially across N detectors or pixels. Our approach employs N tips or gratings that distribute the light temporally against one detector. When detecting intrinsic fluorescence, the detector in this design sees optical signals in the pW to nW range. As a result, the detector must have a high gain-bandwidth product. Detectors with internal gain (PMTs at 10^5, EMCCDs at 10^3, and APDs at 50) are of interest because they can amplify low-level signals above read-out and/or preamp noise. To obtain a useful signal-to-noise ratio (SNR), our system uses a fiber coupled PMT with 10^9 V/W at 6 MHz. In most existing confocal instruments, only one or a small number of wavelengths can be measured during each spatial scan. High-end systems do offer solutions using 32 PMT elements. Our approach is intended to be more cost effective for clinical applications. SNR is defined as peak signal divided by the RMS noise. Since our system is shot limited, the SNR is driven by signal strength, which in turn is driven by fluorescence yield, collection efficiency, and spectrometer throughput.

Higher collection efficiency is obtained by using a larger confocal aperture. Fiber tip arrays have been fabricated with both 10 micron and 62.5 micron core fiber. Each tip is attached to another fiber with physical contact such that the coatings are immersed between glass on both sides. The larger core provides a 7x improvement with tissue samples. Neither of these core sizes are compatible with fiber gratings for visible wavelengths – which perform optimally with single mode fiber having a 3 micron core diameter. The angular distribution in multimode fiber (MMF) must be assessed regarding operation with coated fiber tips. The angular distribution in MMF is a function of launch conditions.[14] Our confocal optics use low angle injection – i.e. about ± 6 degrees at the confocal aperture. Due to Snell's law, the angle of incidence at a fiber tip within the MMF is therefore about 4 degrees. In comparison, we should mention that the maximal coupling angle is 24° and the maximal internal angle is 15° when a Lambertian source is used to populate all modes in a MMF (NA = 0.4). Figure 2 shows ten identical high pass filters spaced 30 nm apart. The bluest filter is mapped into the first bin and the reddest filter is mapped into the last bin. Modeled spectra show that these curves only move about 2 nm to the blue as the internal angle of incidence increases from zero to 5 degrees.

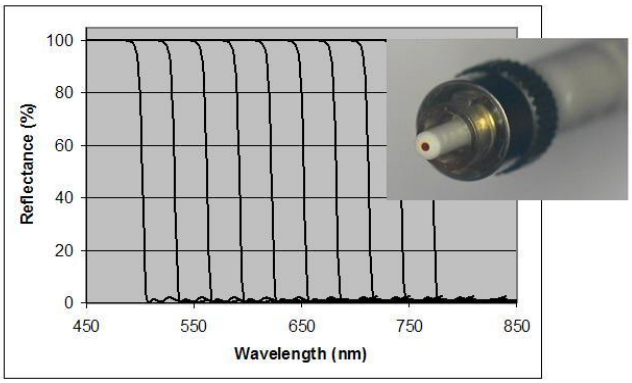

Figure 2. Spectral array of coated fiber tips

The key advantage of this design is speed – a spectrum is acquired during the dwell time of each pixel in the spatial scan. Beyond speed, this new design has several other advantages. First, wavelength bin centers and widths can be arranged in an arbitrary manner with varying widths matched to a given application. Second, the wavelength separation method has no influence on spatial scanning fidelity. A map of a given color will spatially register with a map of another color. Third, each polarization state is reflected in a similar manner. Fourth, the new design is compatible with confocal optics.

2.4 Software and firmware

The optical system described above is controlled by software running on a 1.73 GHz quad-core Intel i7-820 processor, and firmware running on a custom electronics box (see system photo in figure 3). The software, written in LabView, generates the graphical user interface (GUI) shown in figure 4. The firmware runs on board-mounted FPGA and DSP chips within the electronics box, which also provides several interconnects to the optical package and the quad box. These interconnects include the following inputs (start trigger, USB, fiber to PMT), and outputs (scan mirror control signals, laser trigger, PMT analog output, A-to-D start trigger, sampling clock). A 14-bit digitizer card capable of 100 MS/s is mounted within the quad box chassis. Several events occur during operation: the GUI issues a start pulse, the electronics box sends control signals to the laser and mirrors, the digitizer card receives a start pulse, the PMT output, and the sampling clock. The quad box receives a serial array of acquisitions from the digitizer, and casts the data into a three-dimensional datacube.

Selected slices of the data cube and a bin histogram are displayed on the GUI in real time. An example from a scan on mixed quantum dots is shown in figure 4. The GUI includes settings for allocations amongst space, wavelength, and over sampling – which are forwarded via the USB to the electronics box. Default settings are: 200 pixels per line, 150 lines per datacube, 15 spectral bins per pixel, and 10 samples per bin. As indicated in Figure 5, the GUI allows multiple image display modes: any selected spectral bin in grey levels (A), the sum of all selected spectral bins in grey levels (B), three selected spectral bins assigned to RGB levels (C), and any combinations of bins can be entered into formulae to generate RGB levels. These formulae, for example, can assign grey levels to the delta between two bins normalized by a third bin – or a similar computation customized for the red, green and blue levels. An example is given in figure 4 where bin 4 is assigned to red, bin 3 to green, and bin 2 to blue. Our goal is to use multiple bins to colorize an image that clearly shows the presence of abnormal tissue at cellular spatial resolution. The GUI also provides regions-of-interest (ROI) analysis tools, and storage of a sequence of frames from bin 1 to bin N to facilitate development of the colorization formulae.

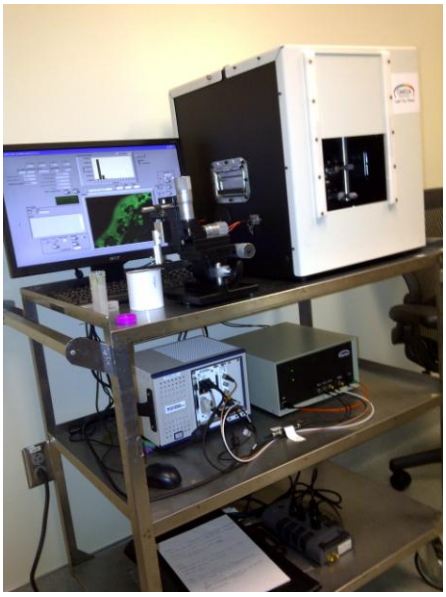

Figure 3. System photo: monitor, optical package, electronics box, quad core controller

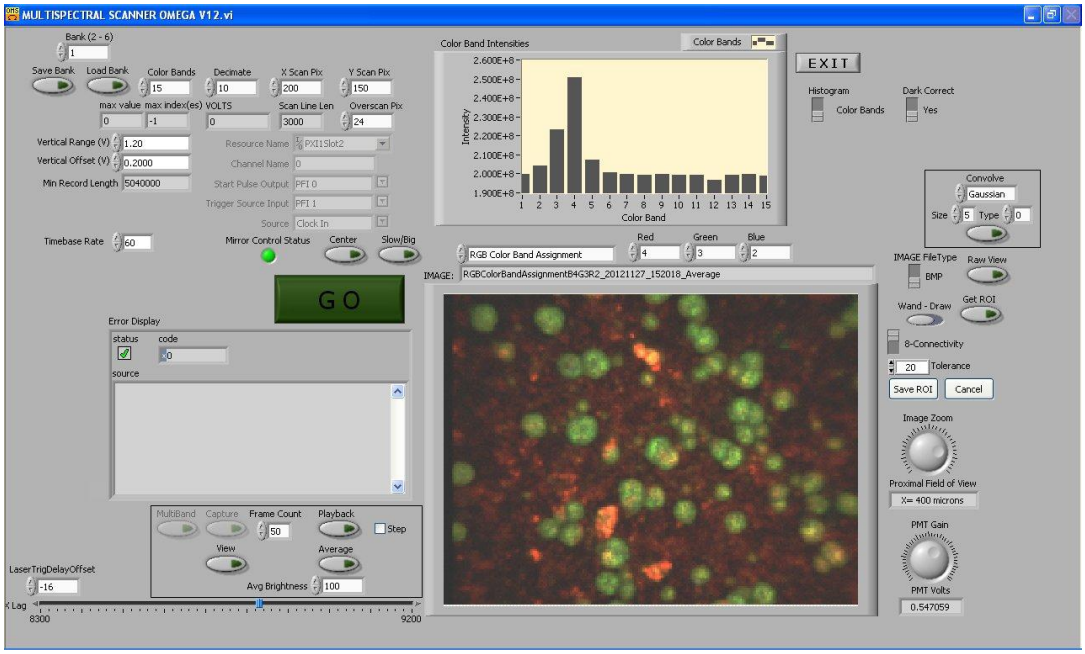

Figure 4. System GUI showing controls, bin histogram, and multispectral image of mixed q-dots (the image contains green colorized round clumps collected in bin 3 and a red colorized background collected in bin 4)

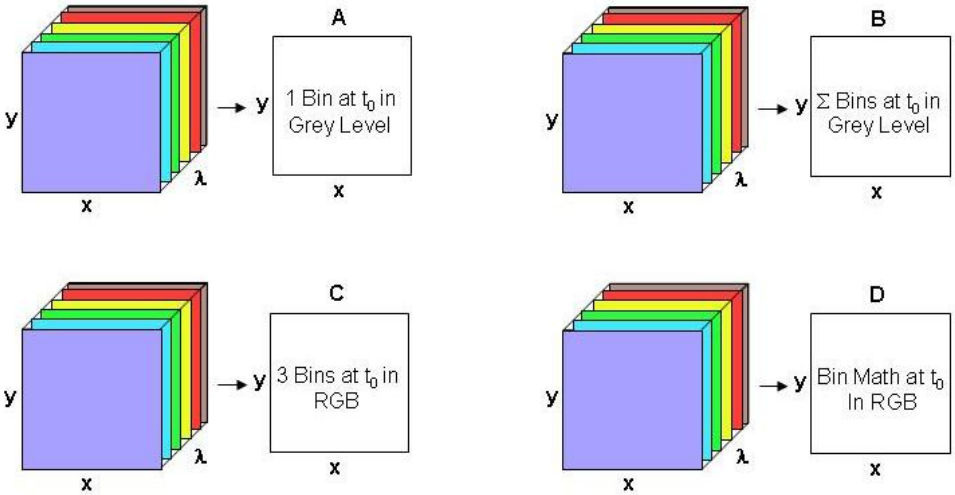

Figure 5. Modes for extracting 2D images from 3D datacubes (all images occur at 10/sec and can be summed or saved as a series of frames over $t_0 - t_N$)

3. RESULTS

At a typical sampling rate of 60 MHz, each image generation mode shown in figure 5 functions at 10 frames per second. This temporal rate is sufficient for avoiding image artifacts caused by a subject's pulse and respiration while diagnosing disease and/or directing surgical margins.

As for spatial resolution, our microscopy mode has observed 1 micron bars on a known test target. Further, figure 6 shows fluorescent beads imaged by both the microscopy and endoscopy modes. The beads were drop cast from solution onto a glass slide, and are 3 microns in diameter. The smallest spots on the microscopy image are individual beads, while the smallest grouping of illuminated fibers in the endoscopy image are individual beads. The endoscopic bundle contains 30,000 fibers, which are packed into a hexagonal array and appear superimposed on the image. An individual fiber represents 0.3 to 0.4 microns in the plane of the tissue. This spatial resolution is sufficient for cellular level analysis.

As for spectral resolution, the microscopy mode has imaged quantum dots with peak emission at 650 nm (CdSe/ZnS powder), 558 nm (CdSe/ZnS powder), and 486 nm (CdSe in toluene). These quantum dots were chosen because they respond to blue excitation and exhibit fairly discrete emission spectra. The dots were suspended in toluene and drop cast onto glass slides. These tests were completed with a 488 nm laser and the following three bins: 506-522 nm, 522-614 nm, and 614-699 nm. An additional test was completed with a 405 nm laser and the bluest bin expanded to 450-522 nm. The binning histograms showed that the spectra for each q-dot appeared in the appropriate bins with expected crosstalk. This data indicates that the mapping of spectral bins into the time domain is functional, and has the potential to distinguish between healthy and abnormal tissue.

Images were taken on fixed rat breast and ex-vivo mouse tissue in microscopy mode using the three spectral bins defined above. All images were adjusted for brightness and contrast. Figure 7 exhibits images (R = 2x bin 4, G = bin 3, B = bin 2) of the fixed, unstained, rat breast tissue. The right breast had been transfected with human breast cancer cells and appears to show spectral differences on the inner duct walls. Figure 8 presents images (R = bin 4, G = bin 3, B = bin 2) of several ex-vivo mouse organs - including heart, lung, liver, spleen, and kidney. These tissues were scanned within minutes of animal death to assess signal strength before various metabolic fluorophores expired. Signals were somewhat dim – requiring the averaging of multiple frames. A more powerful laser is available for addressing this issue while still keeping average power within acceptable limits. This data indicates that our system can generate multispectral images of intrinsic fluorescence from several animal organs.

In-vivo studies (per IACUC protocols) have been undertaken on preclinical (mouse) models at the Cedars-Sinai Medical Center in Los Angeles. In-vivo imaging of an animal model allows both the disease and the effects of treatment to be studied as they happen, and be quantified in a reproducible way. These results will be reported elsewhere.

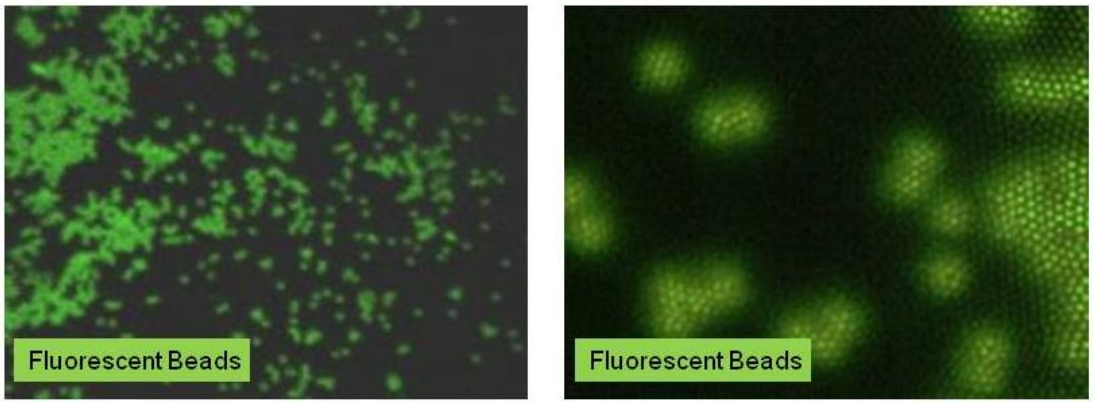

Figure 6. Microscopy mode (left, 200 μm FOV) and endoscopy mode (right, 43 μm FOV)

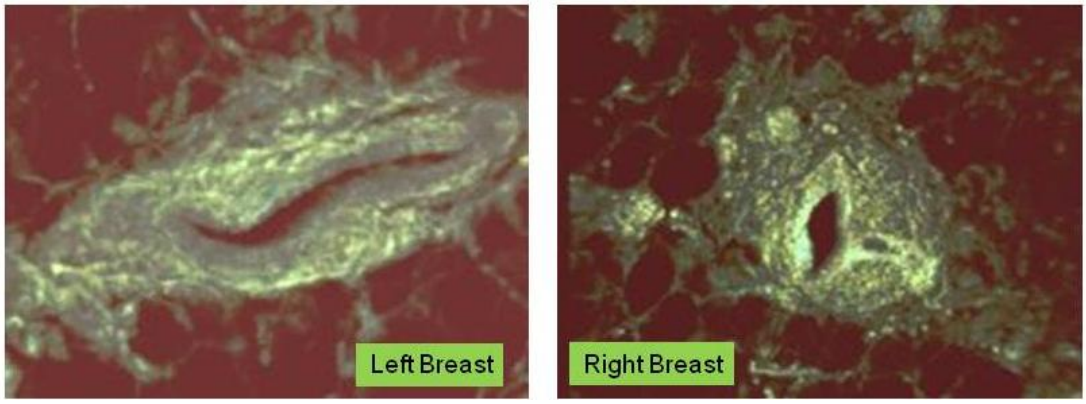

Figure 7. Fluorescence from fixed rat breast (excited with 488 nm, 200 μm FOV)

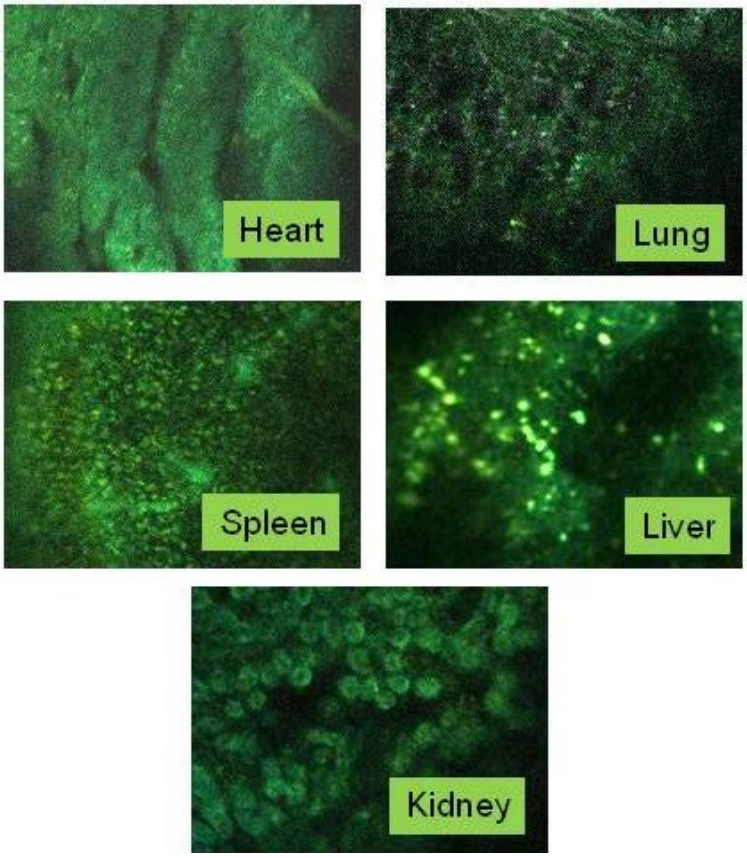

Figure 8. Intrinsic autofluorescence of ex-vivo mouse organs (excited with 488 nm, 200 μm FOV)

4. CONCLUSIONS

The multispectral imaging system described in this paper has been designed, built, and tested for the spectral mapping of intrinsic tissue fluorescence (autofluorescence). The spatial resolution is sufficient for cellular level imaging. The spectral resolution is suitable for detecting the spectral signatures of cancer. The temporal resolution is sufficient for avoiding the cardiovascular and respiratory rhythms of living subjects. The system has been demonstrated on several

samples, including fluorescent beads, quantum dots, fixed tissue, and ex-vivo tissue. The approach is similar to older confocal microscopes that use a rotating filter wheel – except that the filters are effectively rotated at the speed of light. Other systems have more resolution in either space, wavelength, or time - but generally not simultaneously. Our approach is a cost-effective design with resolution appropriate for detecting intrinsic fluorescence in a clinical setting. Our ultimate goal is to enable preventive health and the early detection of disease via optical biopsy. The technique would also allow surgeons to assess surgical margins in real time. For example, our multispectral imaging endoscope could be used in the intraoperative assessment of lumpectomy margins.

The above concepts and designs are applicable to microscopy, endoscopy, and cytometry. One can imagine applications involving fluorescence, two-photon spectroscopy, and Raman spectroscopy with future impact on both cytomics, histomics, and clinical settings.

ACKNOWLEDGEMENTS

We are grateful to Dr. V. Krishnan Ramanujan for his participation, expert help, and advice regarding ongoing in-vivo and ex-vivo studies at the Cedars-Sinai Medical Center in Los Angeles. These results will be jointly published elsewhere. We further thank Dr. Bob Johnson of Omega Optical for supporting this effort.

REFERENCES

[1] Chung, A., Wachsmann-Hogiu, S., Zhao, T., Xiong, Y., Joseph, A., Farkas, D.L., "Advanced optical imaging requiring no contrast agents - A new armamentarium for medicine and surgery," Current Surgery 62, 365-370 (2005).

[2] Zellweger, M., Goujon, D., Conde, R., Forrer, M., van den Bergh, H., Wagnieres, G., "Absolute autofluorescence spectra of human healthy, metaplastic, and early cancerous bronchial tissue *in vivo*," Applied Optics 40(22), 3784-3791 (2001).

[3] Thiberville, L., Moreno-Swirc, S., Vercauteren, T., Peltier, E., Cave, C., Heckly, G.B., "*In Vivo* imaging of the bronchial wall microstructure using fibered confocal fluorescence microscopy," Am J Respir Crit Care Med 175, 22–31 (2007).

[4] Fu, S., Chia, T.C., Kwek, L.C., Diong, C.H., Tang, C.L., Choen, F.S., Krishnan, S.M., "Application of laser induced autofluorescence spectra detection in human colorectal cancer screening," Proc. SPIE-OSA Biomedical Optics 5141, 298-304 (2003).

[5] Ramanujan, V.K., Ren, S., Park, S., Farkas, D.L., "Non-invasive, contrast-enhanced spectral imaging of breast cancer signatures in preclinical animal models i*n vivo*," J Cel Sci Therapy 1, 102-106 (2010).

[6] Carver, G.E., Heebner, R.W., Astfalk, G., "Wafer level testing for semiconductor laser manufacture via spatially resolved photoluminescence," IEEE Journal of Quantum Electronics 1(4), 980-986 (1995).

[7] Farkas, D.L., Ballou, B., Du, C., Fisher, G.W., Lau, C., Niu, W., Wachman, E.S., "Optical image acquisition, analysis and processing for biomedical applications" Springer Lecture Notes in Computer Science 1311, 663-671 (1997).

[8] Vogel, A., Venugopalan, V., "Mechanisms of pulsed laser ablation of biological tissues," Chem.Rev. 103, 577-644 (2003).

[9] Pawley, J.B., [Handbook of Biological Confocal Microscopy, 2nd Ed.], Plenum Press, New York, (1995).

[10] Cremer, T., Kreth, G., Koester, H., Fink, R.H.A., Heintzmann, R., Solovci, I., Zink, D., "Chromosome territories, interchromatin domain compartment and nuclear matrix: An integrated view of the functional nuclear architecture," Critical Review in Eukaryotic Gene Expression 12 (2), 179-212 (2000).

[11] Carver, G.E., "Scanned photoluminescence with high spatial resolution in semi-insulating GaAs and InP: aspects of surface passivation and photodegradation," Semicond. Sci. Technol. 7, A53-A58 (1992).

[12] Udovich, J.A., Kirkpatrick, N.D., Kano, A., Tanbakuchi, A., Utzinger, U., Gmitro, A.F, "Spectral background and transmission characteristics of fiber optic imaging bundles," Applied Optics 47(25), 4560-4568 (2008).

[13] Carver, G.E., Farkas, D.L., Porque, J., Feder, K.S., Westbrook, P.S., "Visible wavelength fiber Bragg grating arrays for high speed biomedical spectral sensing," in Bragg Gratings, Photosensitivity and Poling in Glass Waveguides, OSA Technical Digest, paper BThB5 (2010).

[14] Midwinter, J.E., [Optical Fibers for Transmission], John Wiley & Sons, Inc., New York, 204-205 (1979).